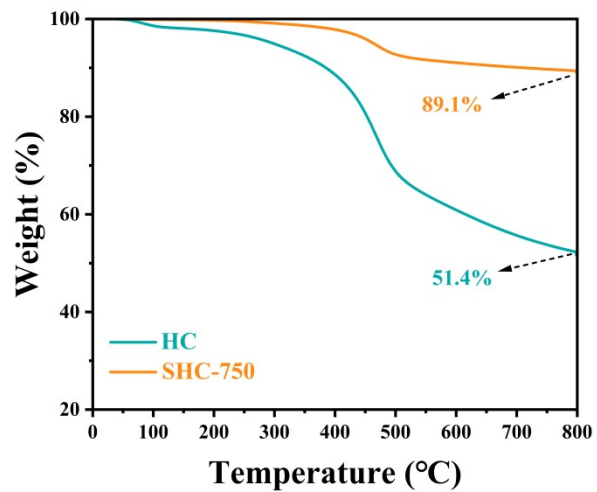


*Supporting Information for:*

**Achieving High-Capacity Sodium Insertion of Coal-based Hard Carbon Anodes  
via Closed-Pore Modification**



**Figure S1** TG curves of HC and SHC-750

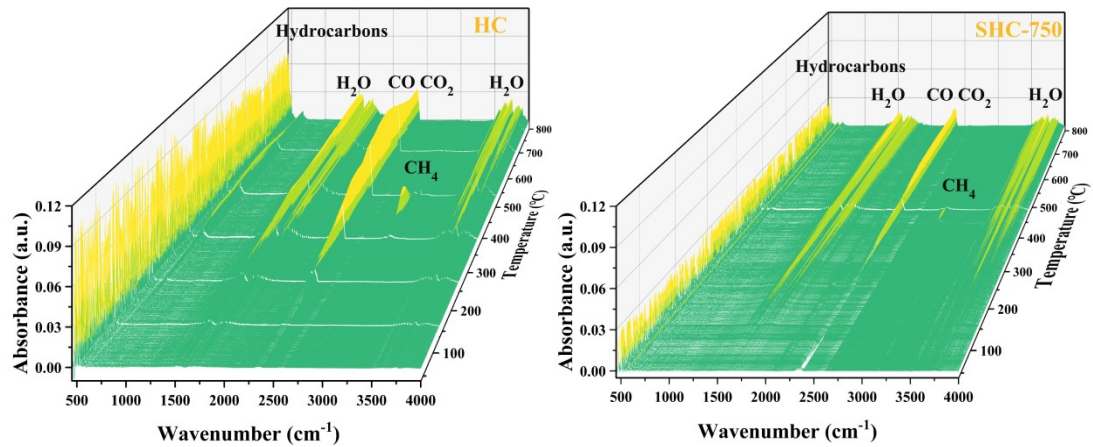
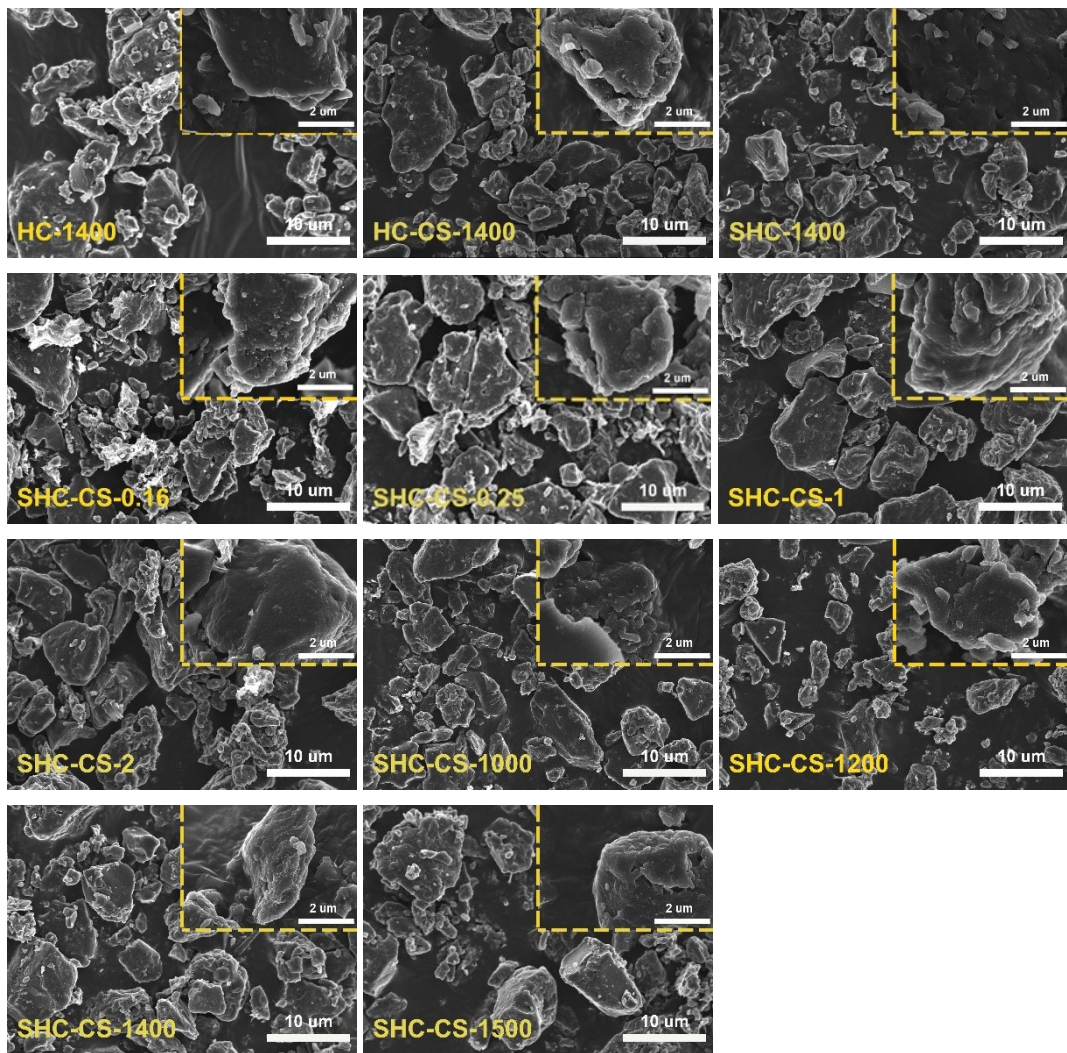
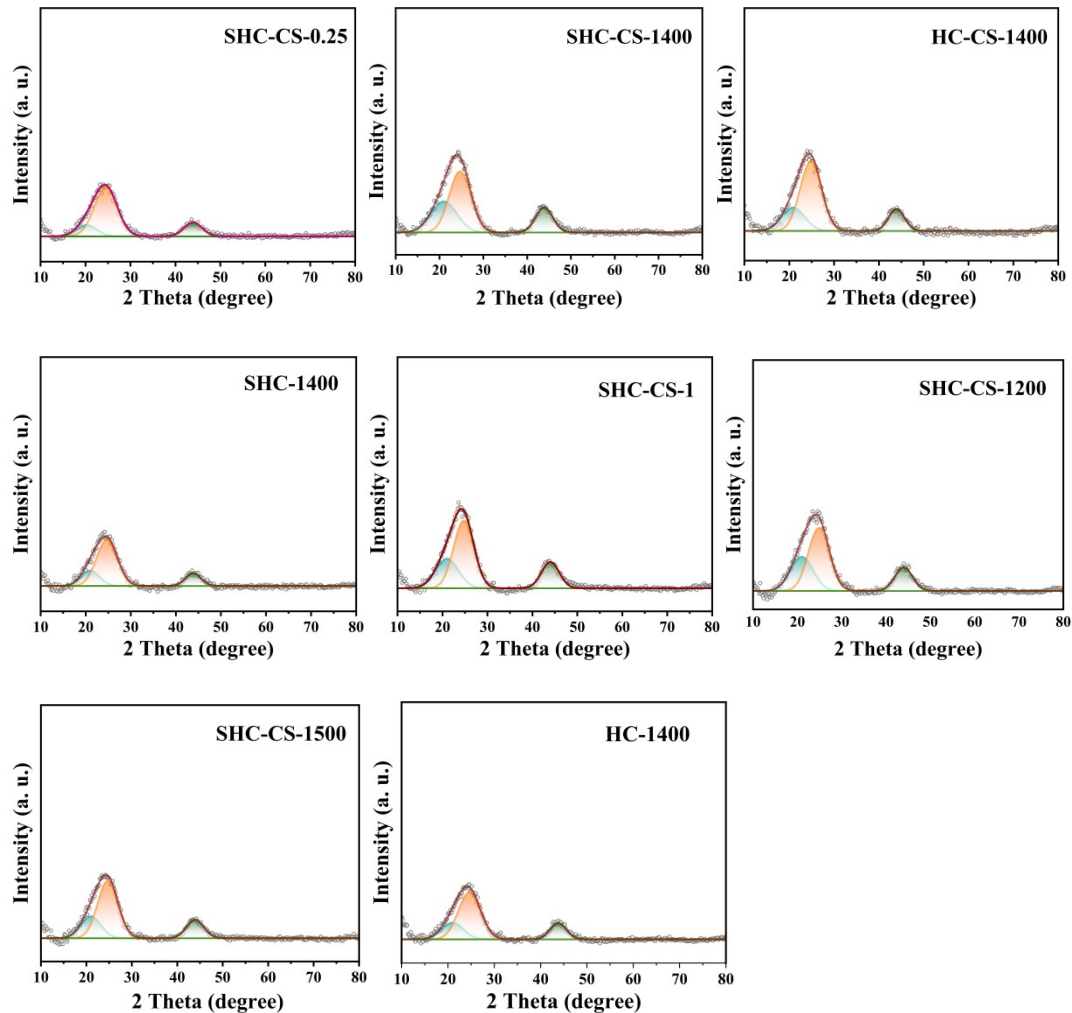


Figure S2 (a)HC, (b)SHC-750 的 TG-FTIR spectrum



**Figure S3** The SEM images of HC samples. SEM images of (a) HC-1400, (b) HC-CS-1400, (c) SHC-1400, (d) SHC-CS-0.16, (e) SHC-CS-0.25, (f) SHC-CS-1, (g) SHC-CS-2, (h) SHC-CS-1000, (i) SHC-CS-1200, (j) SHC-CS-1400and (k) SHC-CS-1500 samples.



**Figure S4** The fitting results of XRD patterns of (a) SHC-CS-0.25, (b) SHC-CS-1400, (c) HC-CS-1400, (d) SHC-1400, (e) SHC-CS-1, (f) SHC-CS-1200, (g) SHC-CS-1500 and (h) HC-1400 samples.

$$d = \frac{\lambda}{2 \times \sin(\theta_{002})}$$

Where  $\lambda$  is the wavelength of the X-rays (0.154178 nm),  $2\theta_{002}$  is the peak position of (002) peak in the XRD pattern.  $K_{Cu} = 0.15406$  nm.

$$La = 1.84\lambda/B_{100}\cos\theta_{100}$$

$$Lc = 0.89\lambda/B_{002}\cos\theta_{002}$$

Where  $\lambda$  is the wavelength of the X-rays (0.154178 nm),  $B_{100}$  and  $B_{002}$  are the full width at half maxima of the (100) and (002) peaks,  $2\theta_{100}$  and  $2\theta_{002}$  are the corresponding peak positions.

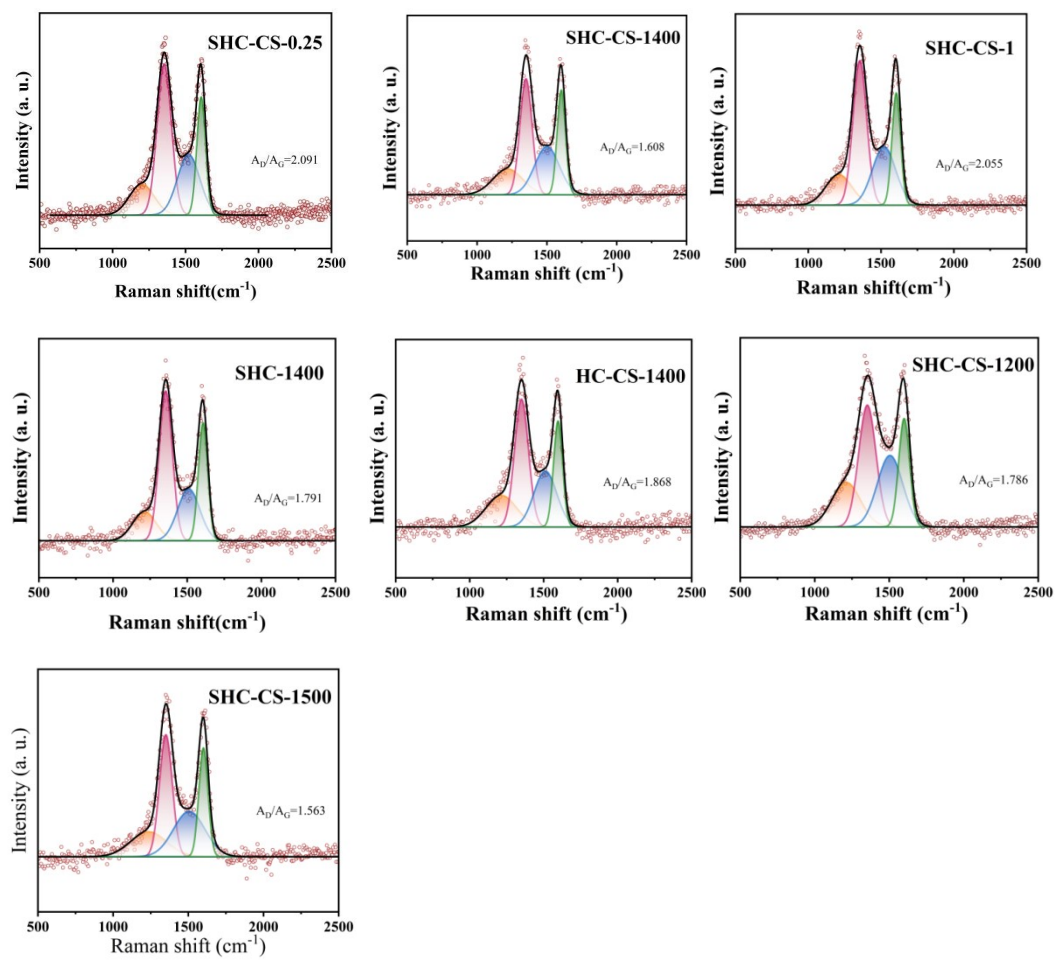


**Figure S5** The fitting results of Raman spectra of (a) SHC-CS-0.25, (b) SHC-CS-1400, (c) SHC-CS-1, (d) SHC-1400, (e) HC-CS-1400, (f) SHC-CS-1200, and (g) SHC-CS-1500 samples.

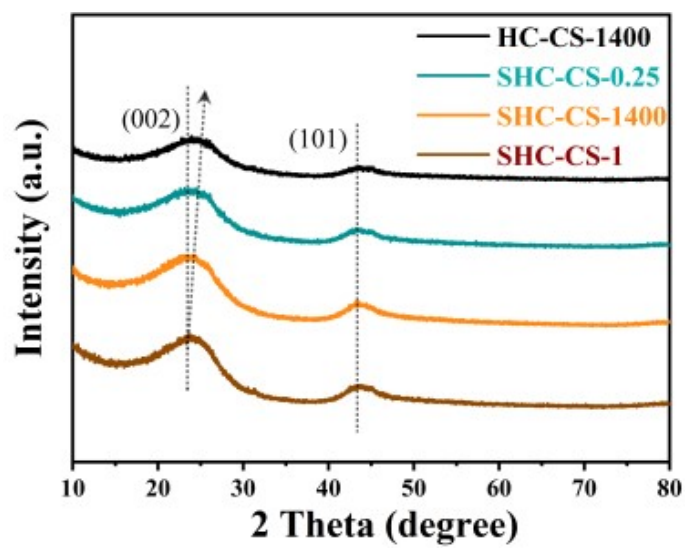


**Figure S6** XRD patterns of HC samples with different CS ratios.

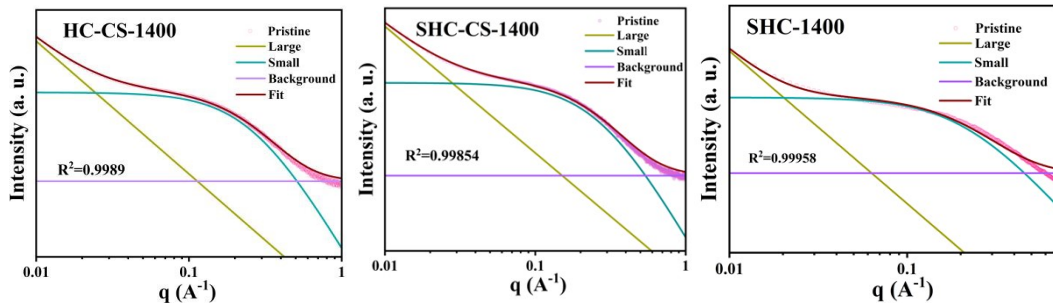


**Figure S7** Fitted SXAS patterns of HC samples.

The scattered intensity from a medium containing nanopores together with macropores can be represented by the function:

$$I(q) = \frac{A}{q^a} + \frac{B a_1^4}{(1 + a_1^2 q^2)^2} + D$$

Where  $q$  is the wavevector,  $A$  and  $B$  are proportional to the total surface areas of the large and small pores, and  $D$  is a constant background term. the radius of a spherical pore equivalent to Debye's length, is  $R = a_1 \sqrt{10}$

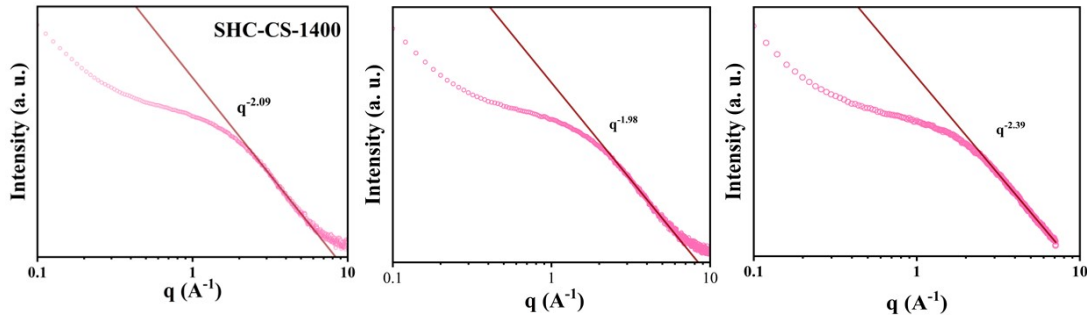


**Figure S8** Porod fitted SXAS patterns of HC samples.

A power law fit in this region of the scattering curve,  $I(q)=A*q^{-n}$  ( $q = 3\sim6 \text{ nm}^{-1}$ ), is applied to access pore surface and surface roughness.  $A$  is the Pollard constant proportional to the inner surface and  $n$  is the power exponent. The  $n$  is related to the surface roughness of the nanopore. A larger value indicates a smoother surface.

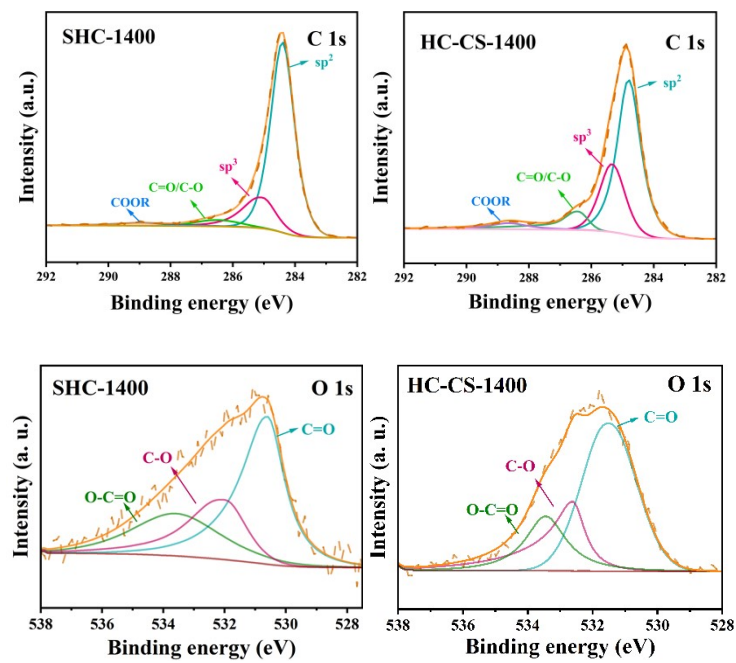


**Figure S9** The high-resolution C 1s XPS spectra of (a) SHC-1400, (b) HC-CS-1400; The high-resolution O 1s XPS spectra of (c) SHC-1400 (d) HC-CS-1400.

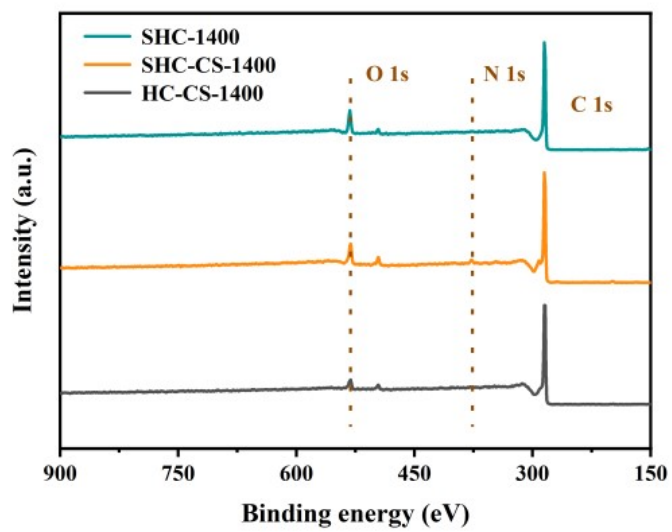


**Figure S10** XPS full spectrum of HC samples: SHC-1400, SHC-CS-1400, HC-CS-1400.

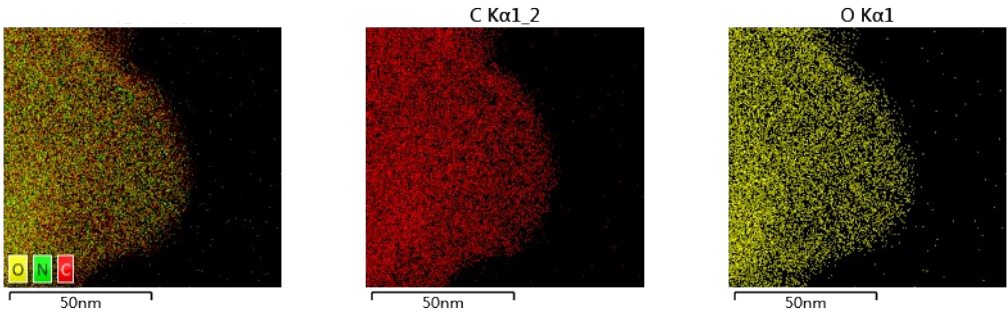


**Figure S11** EDS of SHC-CS-1400

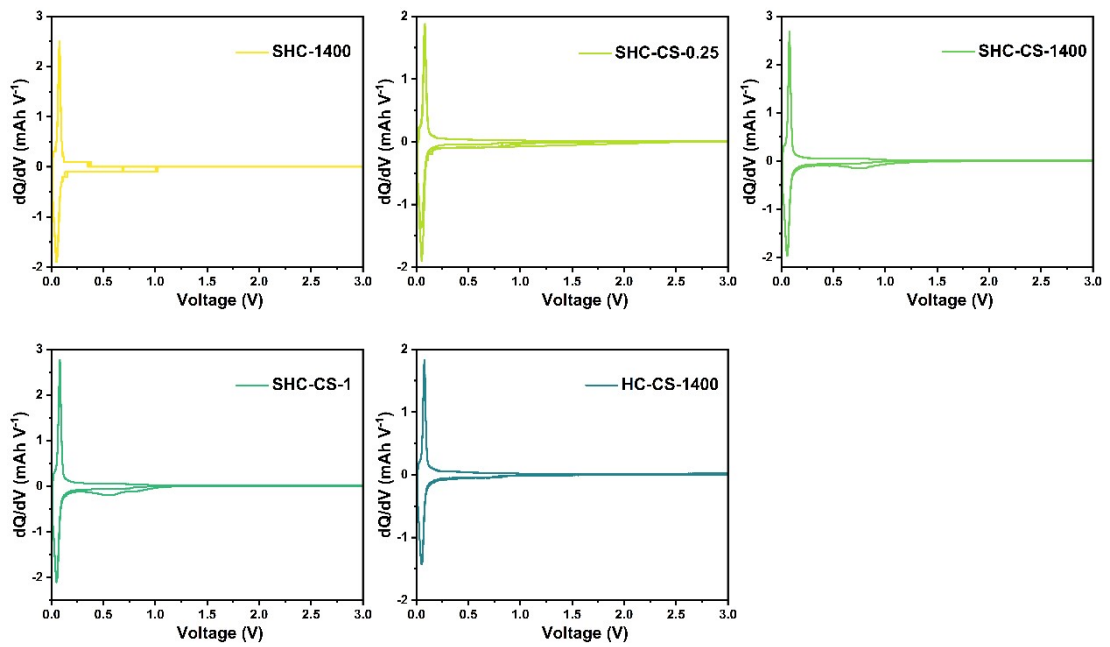


**Figure S12** The dQ/dV curves of HC samples.

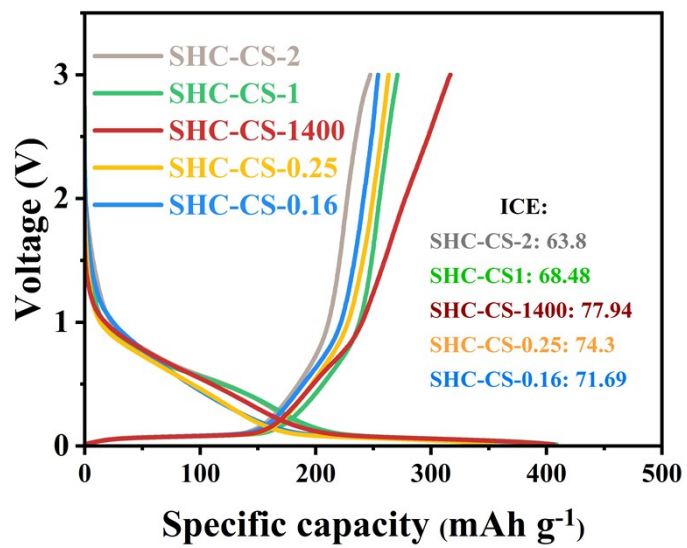


**Figure S13** GCD curves of SHC-CS-2, SHC-CS-1, SHC-CS-1400, SHC-CS-0.25, SHC-CS-0.16.

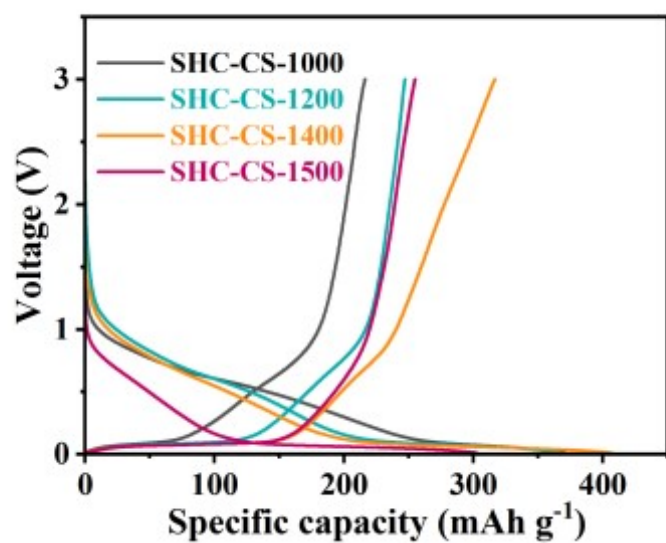


**Figure S14** GCD curves of samples treated at different temperatures

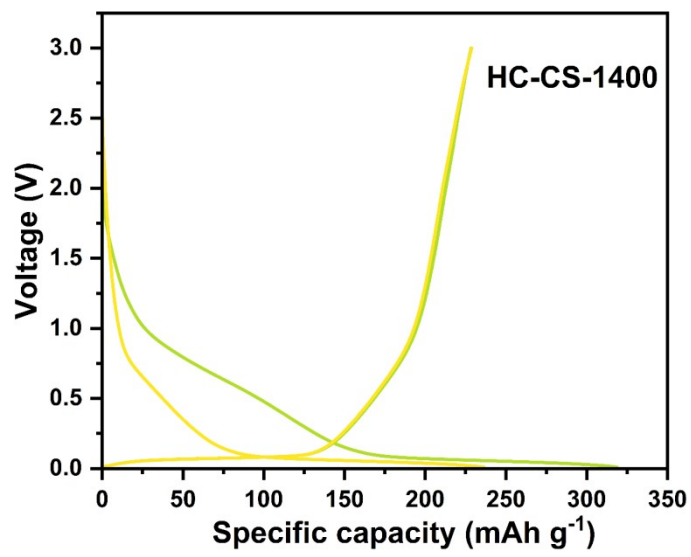


**Figure S15** GCD curves of HC-CS-1400.

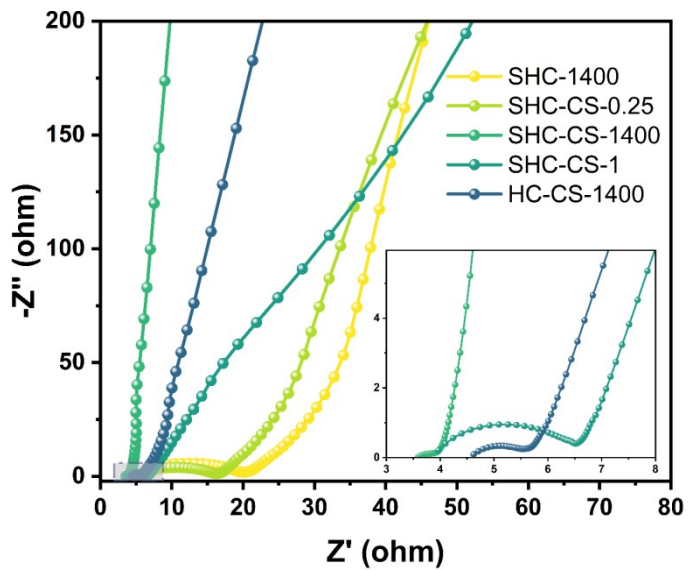


**Figure S16** EIS results of HC electrodes at initial open-circuit voltage

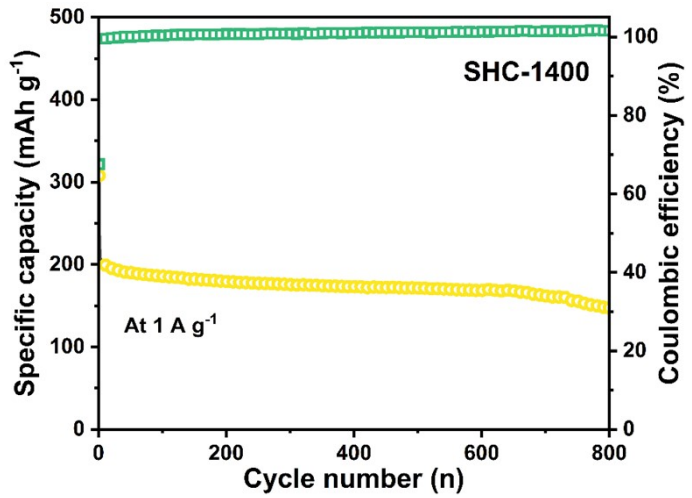


**Figure S17** Cycling performance of SHC-1400 at 1A g<sup>-1</sup> current density

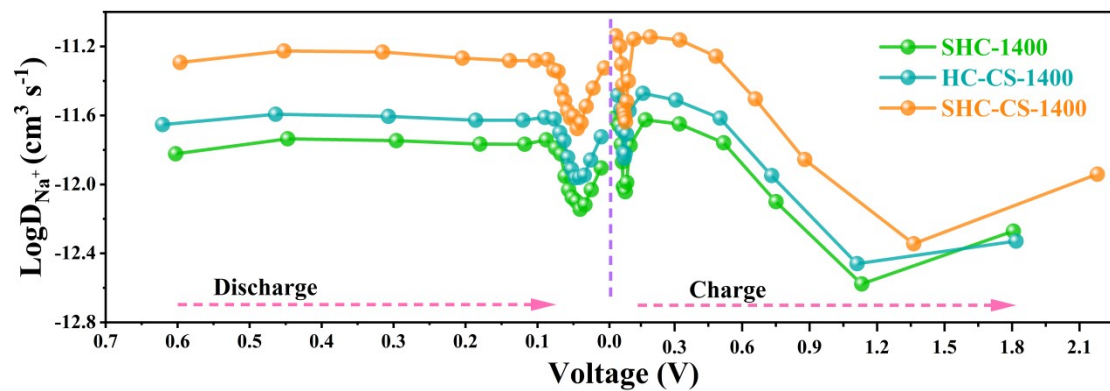


**Figure S18** GITT curves of SHC-1400, HC-CS-1400 and SHC-CS-1400

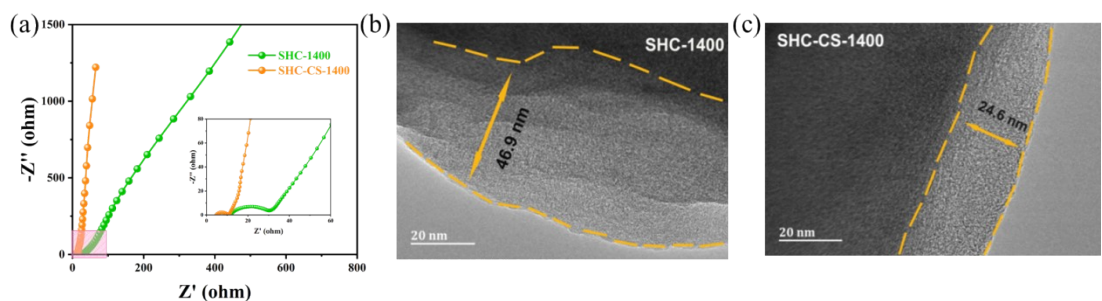


**Figure S19** (a) EIS curves for the SHC-1400 and SHC-CS-1400 anode after cycling, HRTEM images of the SEI from (b) SHC-1400 and (c) SHC-CS-1400 anodes



**Figure S20** Optical photographs of (a) HC-CS-1400, (b) SHC-1400 and (c) SHC-CS-1400 electrodes immersed in an ethanol solution containing phenolphthalein at different discharge stages

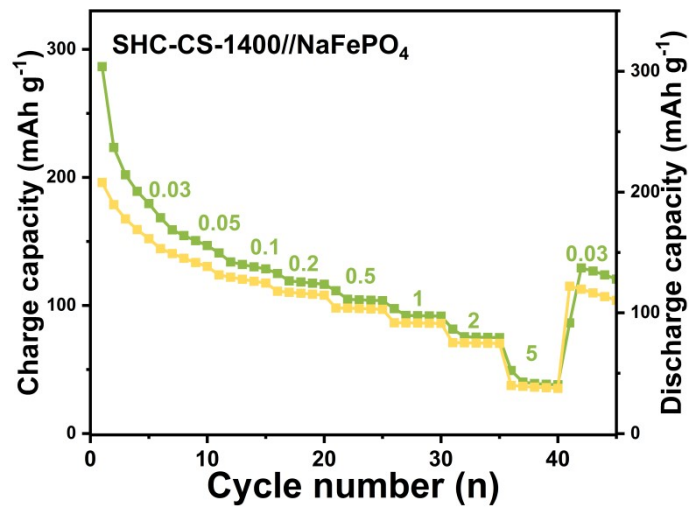


**Figure S21** The rate capability of SHC-CS-1400//NaFePO<sub>4</sub>.

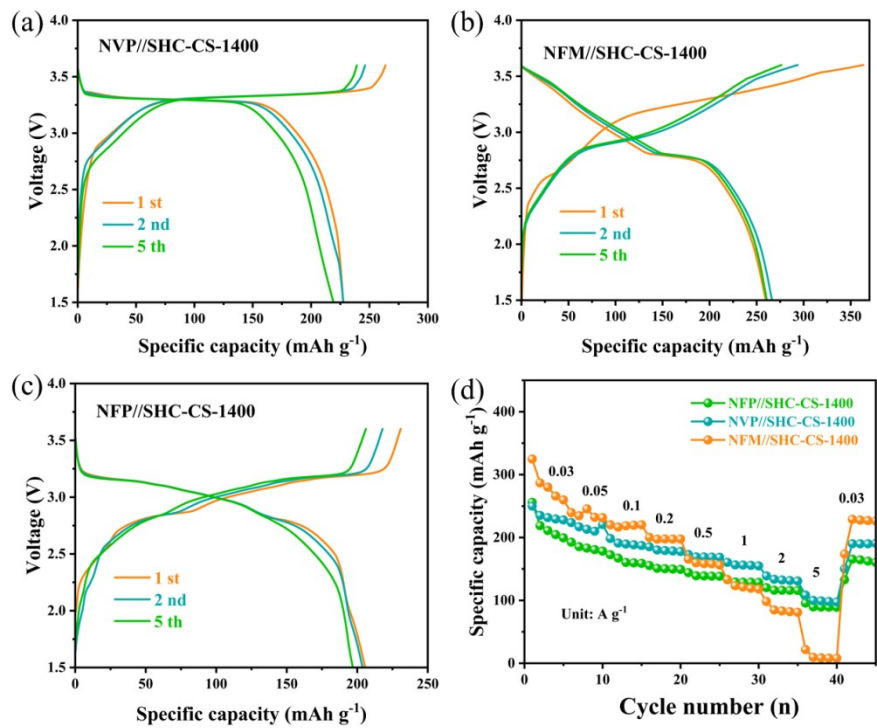


**Figure S22** (a) 1st, 2nd, and 5th turn GCD curves of (a) NVP//SHC-CS-1400, (b) NFM//SHC-CS-1400, and (c) NFP//SHC-CS-1400; and (d) rate capability of the full battery

**Table S1** Physicochemical properties of HC samples

sample	$2\theta_{002}$	$d_{002}$	R	$2\theta_{100}$	$B_{100}$	$L_a$	$B_{002}$	$L_c$	$I_D/I_G$	$A_D/A_G$
SHC-1400	23.88	0.372	/	43.47	3.640	4.807	5.728	1.403	1.202	1.791
SHC-CS-0.25	23.98	0.371	2.027	43.34	3.923	4.458	5.909	1.360	1.191	2.091
SHC-CS-1400	23.51	0.378	2.049	43.46	3.944	4.436	6.355	1.264	1.132	1.608
SHC-CS-1	23.77	0.374	2.129	43.79	3.986	4.395	5.853	1.373	1.103	2.055
HC-CS-1400	24.54	0.362	/	43.72	3.827	4.576	6.027	1.335	0.997	1.868
HC-1400	24.09	0.369	/	43.23	3.587	4.874	5.848	1.375	/	/
SHC-CS-1200	23.62	0.376	2.125	43.99	4.081	4.296	6.370	1.261	1.234	1.786
SHC-CS-1500	24.10	0.369	2.042	43.27	3.861	4.529	5.670	1.418	1.169	1.563

**Table S2** Porosity information of HC samples

sample	SSA <sub>BET</sub> , N <sub>2</sub> /m <sup>2</sup> g <sup>-1</sup>	V <sub>N<sub>2</sub></sub> , <300 nm/cm <sup>3</sup> g <sup>-1</sup>	True density /g mL <sup>-1</sup>	V <sub>closed</sub> pore	D <sub>closed</sub> pore /nm	n
SHC-1400	1.8102	0.005635	1.916	0.07951	1.489	2.390
SHC-CS-1400	0.8770	0.006036	1.827	0.1050	1.219	2.093
HC-CS-1400	1.849	0.004025	1.736	0.1334	1.193	1.980

**Table S3** Electrochemical data of samples treated at different temperatures

Samples	Charge-specific Capacity (mA h g <sup>-1</sup> )	Discharge-specific Capacity (mA h g <sup>-1</sup> )	Initial Coulombic Efficiency (%)
SHC-CS-1000	216.30	370.82	58.33
SHC-CS-1200	232.05	340.11	68.49
SHC-CS-1400	316.75	406.38	77.94
SHC-CS-1500	255.04	302.52	84.31

**Table S4** Comparison of electrochemical performance of SHC-CS-1400 anode with other coal-based anode materials for sodium ion storage reported in previous literatures

Number	Current density (mA/g)	ICE (%)	Specific capacity (mAh/g)	Current density (mA/g)	Specific capacity (mAh/g)	Material	Reference
1	0.03	77.8	316	5	203.	Coal	This work
2	0.05	85.3	312.2	1	106.1	Coal	1
3	0.02	79.5	291	0.4	~50	Subbituminous coal	2
4	0.02	64	200	1	58.2	Coal	3
5	0.02	82.82	300.83	5	140	Coal pitch tar	4
6	0.05	80	278.2	1	207.3	Anthracite coal	5
7	0.037	82.3	308.4	0.6	95	Coal	6
8	0.03	82.9	356	1	100	Lignite coal	7
9	0.02	66	330	5	164	Coal pitch	8
10	0.05	74.2	282	2	130	Anthracite	9
11	0.037	67.5	276.8	0.6	87	Coal tar pitches	10
12	0.02	48.1	284.4	1	61.1	Subbituminous coal	11
13	0.1	55.87	212.3	5	94	Coal	12
14	0.03	74.8	274.2	2	~50	Bituminous coal	13

**Table S5** Comparison of the fast-charging performance of SHC-CS-1400 with other HC materials previously reported in the literature for sodium-ion storage

Number	name	Current density (A/g)	Specific capacity (mAh/g)	Material	Reference
1	BC/R-HC	5	~135	resin	14
2	C—S/C=S	5	254	polydopamine	15
3	RHC	8	109	bamboo powder	16
4	HC-DB	5	~100	bamboo	17
5	HHC	2	83	polystyrene	18
6	M-1500	2	190	wood	19
7	PO-SC-S	3	125	petroleum residue	20
8	CMAC	0.6	70	polypropylene	21
9	HCMP-CO <sub>2</sub>	0.8	171	starch	22
10	TDT	5	215	TDT	23
11	PCHC-10	0.6	103	resin	24
12	SHC-CS-1400	5	203	coal	This work

## References

- [1] H. Chen, N. Sun, Y. Wang, R. A. Soomro, B. Xu. Energy Storage Mater., 2023, 56, 532-541.
- [2] H. Lu, S. Sun, L. Xiao, J. Qian, X. Ai, H. Yang, A. H. Lu, Y. Cao. ACS Appl. Energy Mater., 2019, 2, 729-735.
- [3] L. Deng, Y. Tang, J. Liu, Y. Zhang, W. Song, Y. Li, L. Liu. Molecules, 2023, 28, 4921.
- [4] Y. Wang, N. Xiao, Z. Wang, H. Li, M. Yu, Y. Tang, M. Hao, C. Liu, Y. Zhou, J. Qiu. Chem. Eng. J., 2018, 342, 52-60.
- [5] L. Quan, G. Yunzhi, W. Huiying. New Journal of Chemistry, 2022, 46, 13575-13581.
- [6] K. Wang, F. Sun, H. Wang, D. Wu, Y. Chao, J. Gao, G. Zhao. Adv. Funct. Mater., 2022, 32, 2203725.
- [7] H. Chen, N. Sun, Q. Zhu, R. A. Soomro, B. Xu. Advanced Science, 2022, 9, 2200023.
- [8] W. Sun, Q. Sun, R. Lu, M.-X. Wen, C. Liu, J.-L. Xu, Y.-X. Wu. J. Alloys Compd., 2021, 889, 161678.

- [9] R. Li, B. Yang, A. Hu, B. Zhou, M. Liu, L. Yang, Z. Yan, Y. Fan, Y. Pan, J. Chen, T. Li, K. Li, J. Liu, J. Long. *Carbon*, 2023, 215, 118489.
- [10] L. Ji, Y. Zhao, L. Cao, Y. Li, C. Ma, X. Qi, Z. Shao. *J. Mater. Chem. A*, 2023, 11, 26727-26741.
- [11] W. Song, Y. Tang, J. Liu, S. Xiao, Y. Zhang, Y. Gao, C. Yang, L. Liu. *J. J. Alloys Compd.*, 2023, 946, 169384.
- [12] R. Liu, Y. Li, C. Wang, N. Xiao, L. He, H. Guo, P. Wan, Y. Zhou, J. Qiu. *Fuel Process. Technol.*, 2018, 178, 35-40.
- [13] Z. Lou, H. Wang, D. Wu, F. Sun, J. Gao, X. Lai, G. Zhao. *Fuel*, 2022, 310, 122072.
- [14] K. Wang, M. Li, Z. Zhu, W. Ai, H. Wu, B. Wang, P. He, D. Xie, J. Wu, W. Huang. *Nano Energy*, 2024, 124, 109459.
- [15] H. Feng, Z. Liu, F. Wang, L. Xue, L. Li, C. Ye, C. Zhang, Q. Liu, J. Tan. *Adv. Funct. Mater.*, 2024, 2400020.
- [16] C. Wu, Y. Yang, Y. Zhang, H. Xu, W. Huang, X. He, Q. Chen, H. Dong, L. Li, X. Wu, S. Chou. *Angew Chem Int Edit*, e202406889.
- [17] Y. Wang, Z. Yi, L. Xie, Y. Mao, W. Ji, Z. Liu, X. Wei, F. Su, C.-M. Chen. *Adv. Mater.*, 2401249.
- [18] Y. Qiu, G. Jiang, Y. Su, X. Zhang, Y. Du, X. Xu, Q. Ye, J. Zhang, M. Ban, F. Xu, H. Wang. Hybrid hard carbon framework derived from polystyrene bearing distinct molecular crosslinking for enhanced sodium storage. *Carbon Energy*, e479.
- [19] Z. Tang, R. Zhang, H. Wang, S. Zhou, Z. Pan, Y. Huang, D. Sun, Y. Tang, X. Ji, K. Amine, M. Shao. *Nat. Commun.*, 2023, 14, 6024.
- [20] F. Xie, Y. Niu, Q. Zhang, Z. Guo, Z. Hu, Q. Zhou, Z. Xu, Y. Li, R. Yan, Y. Lu, M.-M. Titirici, Y.-S. Hu. *Angew Chem Int Edit*, 2022, 61, e202116394.
- [21] S. Zhang, N. Sun, X. Li, R. A. Soomro, B. Xu. *Energy Storage Mater.*, 2024, 66, 103183.
- [22] Z. Zheng, S. Hu, W. Yin, J. Peng, R. Wang, J. Jin, B. He, Y. Gong, H. Wang, H. J. Fan. *Adv. Energy Mater.*, 2024, 14, 2303064.
- [23] Y. Yao, M. Pei, C. Su, X. Jin, Y. Qu, Z. Song, W. Jiang, X. Jian, F. Hu. *Small*, 2401481.
- [24] D. Sun, L. Zhao, P. Sun, K. Zhao, Y. Sun, Q. Zhang, Z. Li, Z. Ma, F. Zheng, Y. Yang, C. Lu, C. Peng, C. Xu, Z. Xiao, X. Ma. *Adv. Funct. Mater.*, 2403642.